ANTIOXIDANTS & REDOX SIGNALING
Volume 8, Numbers 7 & 8, 2006

Forum Original Research Communication

A Computational Model for Free Radicals Transport in the Microcirculation

MAHENDRA KAVDIA

ABSTRACT

Nitric oxide (NO), superoxide (O_2^-), and peroxynitrite ($ONOO^-$) interactions in pathophysiologic conditions such as cardiovascular disease, hypertension, and diabetes have been studied extensively *in vivo* and *in vitro*. A reduction in bioavailability of NO is a common event that is known as the endothelial dysfunction in these conditions. Despite intense investigation of NO biotransport and O_2^- and $ONOO^-$ biochemical interactions in vasculature, we have very little quantitative knowledge of distributions and concentrations of NO, O_2^-, and $ONOO^-$ under normal physiologic and pathophysiologic conditions. Based on fundamental principles of mass balance, vessel geometry, and reaction kinetics, we developed a mathematical model of these free radicals transport in and around an arteriole during oxidative stress. We investigated the role of O_2^- and $ONOO^-$ in inactivating vasoactive NO. The model predictions include (a) NO interactions with oxygen, O_2^-, and $ONOO^-$ have relatively little effect on the NO level in the vascular smooth muscle under physiologic conditions; (b) superoxide diffuses only a few microns from its source, whereas peroxynitrite diffuses over a larger distance; and (c) reduced superoxide dismutase levels significantly increase O_2^- and peroxynitrite concentrations and decrease NO concentration. Model results indicate that the reduced NO bioavailability and enhanced peroxynitrite formation may vary depending on the location of oxidative stress in the microcirculation, which occurs at diverse vascular cell locations in diabetes, aging, and cardiovascular diseases. The results will have significant implications for our understanding of these free radical interactions in physiologic and pathophysiologic conditions resulting from endothelial dysfunction. *Antioxid. Redox Signal.* 8, 1103—1111.

INTRODUCTION

NITRIC OXIDE (NO), REACTIVE OXYGEN SPECIES (ROS), and reactive nitrogen species (RNS) are involved in numerous physiologic functions and pathologic conditions (9). NO is generated via the enzymatic oxidation of L-arginine to L-citrulline by several isoforms of NO synthase enzymes (1). NO plays a role in an autocrine and paracrine manner in physiologic processes such as blood pressure regulation, neurotransmission, immunologic response, and inflammation (17,31). *In vivo*, ROS formation is a necessary event resulting from oxygen metabolism, and RNS are produced by interaction of NO with oxygen or ROS. ROS and RNS can interact with DNA, lipids, proteins, and other cellular components and inflict oxidative damage. From bacteria to mammals, organisms have primary and secondary protection mechanisms, such as antioxidants and enzyme systems, to counteract ROS and RNS. However, an excess formation of ROS and RNS at the levels that cannot be adequately counteracted has been implicated in pathogenesis of many diseases, including atherosclerosis, diabetes, and cardiovascular disease.

Endothelial cells (ECs) form the inner lining of vascular lumen and play an important role in the regulation of vascular tone by responding to physical forces and humoral mediators with the release of several relaxing and contracting factors. Endothelial NOS (eNOS), which is primarily a membrane-bound enzyme (13), is considered the principal source of bioavailable vascular NO. NO produced by endothelial cell

Biomedical Engineering Program, University of Arkansas, Fayetteville, Arkansas.

diffuses to vascular smooth muscle and to flowing blood, where it rapidly reacts with hemoglobin (Hb) in red blood cells (RBCs). The endothelium-derived NO stimulates (in the smooth muscle cells) its target hemoprotein soluble guanylate cyclase (sGC) that catalyzes the conversion of guanosine triphosphate (GTP) to cyclic guanosine monophosphate (cGMP) thus relaxing smooth muscle cells and causing vasodilatation (17).

Under normal physiologic conditions, a small fraction of the inspired oxygen is converted to ROS including superoxide (O_2^-) during oxidative phosphorylation in mitochondria. Enzyme superoxide dismutase (SOD) catalyzes the conversion of superoxide to hydrogen peroxide and molecular oxygen. All vascular cells including endothelial cells, and smooth muscle cells have enzyme systems that produce ROS. The possible enzyme systems for vascular superoxide production include nitric oxide synthase (45), NAD(P)H oxidases (38), and xanthine oxidase (50). Of these enzyme systems, membrane-associated NAD(P)H oxidases are a major source of superoxide in vascular diseases, including cardiovascular disease (12,23).

NO reacts very rapidly with superoxide to form strong oxidant peroxynitrite ($ONOO^-$, an RNS) (2, 24). Once formed, peroxynitrite contributes to cellular dysfunction indirectly by reducing NO bioavailability and initiating a number of pathologic processes including lipid peroxidation, nitration of the protein tyrosine residues, and inhibition of key metabolic enzymes, leading to apoptosis (35, 39). Peroxynitrite also oxidizes tetrahydrobiopterin, an NOS cofactor, to dihydrobiopterin (10, 14), resulting in reduced NO formation.

Many aspects of NO, O_2^-, and $ONOO^-$ interactions in pathophysiologic conditions, such as cardiovascular disease, hypertension, and diabetes, have been studied extensively *in vivo* and *in vitro*. A common event is the reduction in bioactive NO availability in these pathophysiologic conditions. This is known as endothelial dysfunction or impaired vasodilation (5). Studies have reported many hypotheses for the cause of the endothelial dysfunction. Figure 1a shows some of the hypotheses at the endothelial cell level including (a) lower NO formation because of reduced availability of NOS substrates and cofactors; (b) higher ROS formation; (c) higher interactions among NO and ROS, leading to damaging RNS or only reducing NO bioavailability; (d) alterations in cellular signaling; and (e) inability of endogenous antioxidant systems to counteract higher ROS and RNS levels.

Figure 1b shows the factors that can affect the levels of NO, ROS, and RNS in the microcirculation. A complete understanding of NO, ROS, and RNS distribution in the microcirculation will require quantitative assessment of biochemical interactions and transport of these species. Mathematical models based on fundamental principles of mass balance, vessel geometry, and reaction kinetics have provided significant results by analyzing the diffusion reaction of free NO in and around an arteriolar vessel, including effects of NO on O_2 transport and metabolism, NO scavenging by Hb, and sGC activation (20, 25, 46). Recently, two models were developed to understand the interactions of O_2^- and SOD with NO (4, 27) in tissue. More detailed models of NO, O_2^-, and $ONOO^-$ interactions were reported to simulate macrophage-related responses (19, 32, 33).

The important results from the NO transport models in the microcirculation include (a) the effect of luminal red blood cell–free layer was significant in allowing a substantial amount of NO to diffuse outward to the smooth muscle cells despite effective scavenging by RBC hemoglobin, and (b) the reaction rate of NO with Hb (inside RBCs) should be several orders of magnitude lower than that of the free Hb to achieve an abluminal NO concentration high enough to activate sGC. NO concentration required for the half-maximal activation of sGC is 23–100 n*M* (3,7).

Despite intensive investigation of NO biotransport and O_2^- and $ONOO^-$ biochemical interactions in vasculature, we have

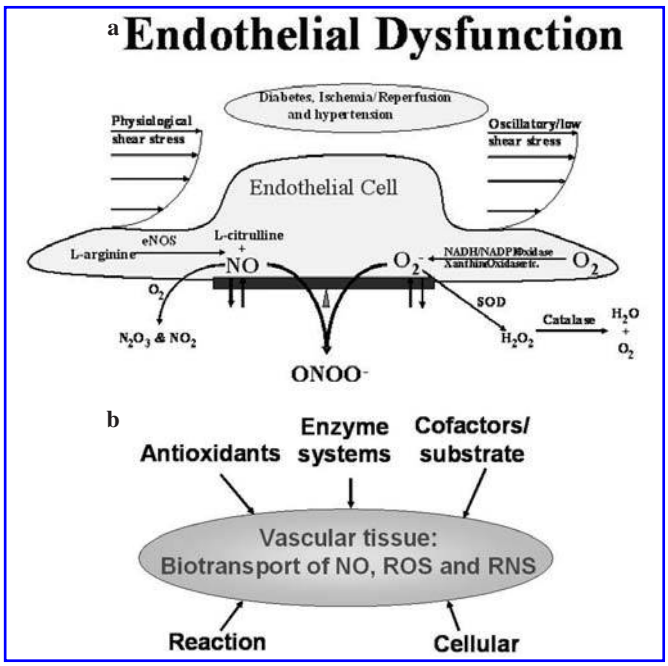

FIG. 1. Interactions and factors affecting NO, ROS, and RNS levels in the microcirculation. Some of the hypotheses at the endothelial cell level for endothelial dysfunction or the reduction in bioactive NO availability are shown in (**a**). Factors that affect the levels of NO, ROS, and RNS in the microcirculation are shown in (**b**).

very little quantitative knowledge of distribution and concentrations of NO, O_2^-, and $ONOO^-$ in the microcirculation under normal physiologic conditions. In addition, fundamental aspects of NO, O_2^-, and $ONOO^-$ transport and biochemical interactions in the tissue remain poorly understood under pathophysiologic conditions. In this study, we present a free radical (*viz*., NO, O_2^-, and $ONOO^-$) transport model in the microcirculation. The model is used to investigate the role of O_2^- and $ONOO^-$ in inactivating vasoactive NO.

METHODS

Model geometry and governing equations

We model a tissue containing an arteriolar vessel (Fig. 2). Arteriolar blood vessel is divided into seven regions of concentric cylinders: a red blood cell–rich (cr) luminal region and a red blood cell–free (cf) luminal region; an endothelium (en); an interstitial space between the endothelial and smooth muscle cells; a smooth muscle layer (sm); and a small nonperfused parenchymal tissue (npt) region. A parenchymal tissue (pt) region perfused by capillaries is considered beyond the nonperfused parenchymal tissue region. The perfused parenchymal tissue region extends to infinity. The radius, r_i, (where i = cr, cf, en, is, sm, npt, or pt) is at the interface between the respective region and the one adjacent to it, as we move away from the central axis of the arteriole.

The principal source of vascular NO is membrane-bound endothelial NOS. Nitric oxide production by arteriolar endothelium is incorporated as surface NO release in boundary conditions at the luminal and abluminal interfaces of the endothelium. The primary source of vascular superoxide is membrane-associated NAD(P)H oxidases. Superoxide production is incorporated as surface O_2^- release in boundary conditions at the luminal and the abluminal interfaces of the arteriolar endothelium, and an overall O_2^- production is considered in all other regions. Oxidative stresses are increased in many disease conditions, resulting in enhanced O_2^- production in various regions of vasculature. Therefore, other sites of excessive O_2^- production also are considered (description in the Results section). No source of peroxynitrite release exists in vasculature. Peroxynitrite production is based on the interaction of NO and O_2^- in all regions.

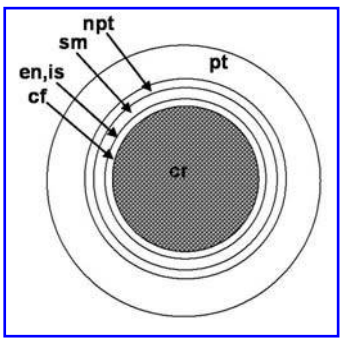

FIG. 2. Model arteriolar geometry. The subregions include luminal RBC-rich region (cr), and RBC-free region (cf); endothelium, (en); interstitial space (is); smooth muscle (sm); and nonperfused (npt) and perfused (pt) parenchymal tissue. Endothelial cell–released NO diffuses into the lumen and to the smooth muscle. In smooth muscle, NO can activate its target enzyme sGC that can relax smooth muscle. NO also can react with superoxide to form peroxynitrite at the location of oxidative stress, and this biochemical interaction is focus of the present study.

A homogeneous solution of RBCs is considered in the RBC-rich luminal region. The capillaries and the parenchymal cells are modeled as a distributed homogeneous medium in the perfused parenchymal tissue region (22).

The convective transport of three species of interest NO, O_2^-, and total peroxynitrite (Per) can be neglected because of their fast reactions (4). Total peroxynitrite is the sum of $ONOO^-$ and peroxynitrous acid (ONOOH), which is an acid form that is in equilibrium with $ONOO^-$ (32). The NO profiles reach steady state within milliseconds (44). Thus, it is appropriate to solve the NO, O_2^-, and Per mass transport in the arteriolar vessel and surrounding tissue by using the steady-state mass-transport equation, written for the cylindrical coordinate

$$D_j \nabla^2 C_j \pm \Sigma R_{j,i} = 0 \tag{1}$$

where j stands for NO, O_2^-, and Per; C_j is the concentration; and D_j is the diffusivity. The net reaction rate, $R_{j,i}$, is the sum of individual reaction rates and production of species j in a region i as described later.

Boundary conditions

At the interfaces, boundary conditions of continuity of NO, O_2^-, and Per flux and concentration are imposed, except for interfaces at (a) the outer edge of the capillary-perfused parenchymal region where a zero-flux boundary condition is applied, and (b) the luminal RBC-free region–endothelium interface (Eq. 2a), and the endothelium–interstitial space (Eq. 2b) interface, where boundary conditions incorporate NO and O_2^- release from the endothelium

$$Q_j = D_j \frac{\partial C_{j,cf}}{\partial r} - D_j \frac{\partial C_{j,en}}{\partial r} \tag{2a}$$

$$Q_j = D_j \frac{\partial C_{j,en}}{\partial r} - D_j \frac{\partial C_{j,is}}{\partial r} \tag{2a}$$

where j represents NO and O_2^-, and Q_j is half of the total NO and O_2^- released by endothelium.

Chemical reactions

The model geometry contains seven separate regions i = cr, cf, en, is, sm, npt, and pt. The most important reactions for our purpose include (a) consumption of NO with Hb contained inside RBCs in luminal RBC-rich regions; (b) oxidation of NO with O_2 in cf, en, is, and npt regions; (c) consumption of NO by sGC in smooth muscle regions; (d) consumption and production of NO by capillaries in parenchymal tissue regions, (e) reaction of NO with O_2^- to yield peroxynitrite in all regions; (f) consumption of O_2^- by super-

oxide dismutase in all regions, and (g) decomposition of peroxynitrite by CO_2 in all regions. The reaction-rate expression for each of these reactions is presented in Table 1.

Parameter values

Model parameter values used for the simulations are presented in Table 1. Rationales for geometric parameters (*e.g.*, wall thickness and radius) are described in detail in our earlier publications (20,21). The r_i (where i = cr, cf, en, is, sm, npt, or pt) are 20.5, 25, 25.5, 26, 32, 62, and 200 μm, respectively. NO, O_2^-, and Per diffusivities of 3.3×10^{-5}, 2.8×10^{-5}, and 2.6×10^{-5} cm^2s^{-1} are assumed (32, 52). Diffusivities were assumed to be the same in all regions.

The production of NO is limited to the arteriolar and capillary wall. We use the half of the total NO release rate (Q_{NO}) of 2.65×10^{-12} mol $cm^{-2}s^{-1}$ for both the luminal and the abluminal sides of the arteriolar endothelium based on experimental data by Malinski (29) in rabbit aorta. The same NO production rate per unit surface area for the capillary is assumed.

The first-order reaction rate of NO in RBC-rich region (k_{cr}) is 1,270 per second, which is a product of the reported rate of reaction of 1.4×10^5 $M^{-1}s^{-1}$ of NO with RBC hemoglobin (6), a heme concentration of 20.3 m*M* in a single RBC, and a core hematocrit of 0.45. For the capillary-perfused parenchymal tissue region, we assume that NO is consumed by blood flowing in capillaries, and NO is produced by capillary endothelial cells. For this region, R_{NO} is equal to $-k_{cap}C_{NO} + Q_{cap}$, where k_{cap} is the effective NO reaction-rate constant for blood flowing in capillaries in parenchymal tissue and is a function of capillary hematocrit (H_c) and fractional capillary volume. Capillary endothelial cell–released NO (Q_{cap}) in the perfused tissue region is distributed uniformly over the tissue volume. Q_{cap} is a function of capillary radius, capillary endothelial NO release rate, and fractional capillary volume. The estimated Q_{cap} is 8.6×10^{-7} M/s, and k_{cap} is 12.4 per second (20).

Superoxide production is assumed at 20% of the NO production at 1.72×10^{-7} M/s in all regions. In the arteriolar endothelium, O_2^- production is considered at 20% of the surface NO release by the endothelium, which is incorporated in surface boundary conditions, as mentioned earlier.

Peroxynitrite formed by reaction of NO and O_2^- is in equilibrium with ONOOH (32). The fraction, f, is the total peroxynitrite in $ONOO^-$ form, and f is equal to $1/(1 + 10^{pK_{Per\text{-}pH}}$, where K_{Per} (6.75) is the acid dissociation constant (32). We assume a pH of 7.4 in the lumen and a pH of 7.0 in the vascular wall.

Numeric solution

A system of equations resulting from Eq. 1 for each species of interest was solved numerically by using the FlexPDE 4.0 software package (PDESolutions, Inc., Antioch, CA). FlexPDE software has an adaptive meshing algorithm

TABLE 1. MODEL PARAMETERS

Parameter	*Value*	*Units*	*Reference*
Systemic hematocrit	45	%	Text
Capillary hematocrit	30	%	Text
Arteriole radius	25	μm	Text
RBC-free–layer thickness	4.5	μm	(41)
en thickness	0.5	μm	(48)
is thickness	0.5	μm	(22)
sm thickness	6	μm	(15)
npt thickness	30	μm	(20)
O_2 concentration	27	μ*M*	(36)
SOD concentration	1 (0.1)	μ*M*	(4)
CO_2 concentration	1.14 (0.114)	m*M*	
Half NO release rate, Q_{NO}	2.65×10^{-12}	mol $cm^{-2}s^{-1}$	(47)
Half O_2^- release rate, $Q_{O_2^-}$	$0.2\ (2) \times Q_{NO}$	mol $cm^{-2}s^{-1}$	Text
D_{NO}	3.3×10^{-5}	cm^2s^{-1}	(52)
$D_{O_2^-}$	2.8×10^{-5}	cm^2s^{-1}	(32)
D_{ONOO^-}	2.6×10^{-5}	cm^2s^{-1}	(32)
f (= C_{ONOO^-}/C_{Per}) in tissue	0.640		Text
f (= C_{ONOO^-}/C_{Per}) in lumen	0.817		Text
Reaction rates of NO with			
O_2, $-k_{O2}C_{NO}^2\,C_{O2}$	9.6×10^6	$M^{-2}s^{-1}$	(26)
O_2^-, $-k_{Per}C_{NO}C_{O2^-}$	$6.7\ (16) \times 10^9$	$M^{-1}s^{-1}$	(16)
sGC, $-k_{sm}C_{NO}^2$	5×10^4	$M^{-1}s^{-1}$	(47)
RBC	1.4×10^5	$M^{-1}s^{-1}$	(6)
RBC-rich core (CR), $-k_{CR}C_{NO}$	1,270	s^{-1}	Text
Capillaries, $-k_{cap}C_{NO} + Q_{cap}$	$12.4\,C_{NO} - 8.6 \times 10^{-7}$	s^{-1}	Text
Reaction rates of O_2^- with			
SOD, $-k_{SOD}C_{O2^-}C_{SOD}$	1.6×10^9	$M^{-1}s^{-1}$	(11)
Reaction rates of $ONOO^-$ with			
CO_2, $-k_{CO2}C_{CO2}fC_{Per}$	5.6×10^4	$M^{-1}s^{-1}$	(37)
NO, $-k_{NO}C_{NO}fC_{Per}$	9.1×10^4	$M^{-1}s^{-1}$	(34)

that generates a larger number of elements in regions with a steep concentration gradient. For simulations, we used adaptive meshing with a relative accuracy of 0.001.

RESULTS

Steady-state NO, O_2^-, and Per profiles for an arteriolar vessel (base-case)

The model was used to calculate NO, O_2^-, and Per concentrations in and around an arteriolar vessel of 50 μm diameter. Figure 3 shows the simulated steady-state NO, O_2^-, and Per concentration profiles based on parameter values of: a luminal RBC-rich region reaction rate of 1,270 per second; a parenchymal NO reaction rate of $12.4 \times C_{NO} - 8.6 \times 10^{-7}$ *M*/s; the same arteriolar and capillary endothelial cell NO production; an NO and O_2^- release-rate ratio of 0.2 in arteriolar and capillary endothelium; and an O_2^- release rate of 0.17 μMs^{-1} in luminal, interstitial space, smooth muscle, and nonparenchymal tissue regions. As seen, the tissue concentrations of NO, O_2^-, and Per vary in radial direction. The maximal concentrations of these species are in the endothelium. The maximum NO, O_2^-, and Per concentrations are 100.6, 1.5, and 3.8 n*M*, respectively. In the luminal region, the NO and O_2^- concentrations reduce to zero in the RBC-rich region after diffusing through luminal RBC-free region. Per concentration is 0.5 n*M* at the center of a lumen. In the vascular wall, the NO, O_2^-, and Per concentrations reach steady-state values of 66.3, 0.1, and 0.9 n*M*, respectively, within 100 μm from the center of the vessel.

Figure 3 also shows the NO profile in the absence of O_2^- production without $ONOO^-$. For this case, the maximum NO concentration is 108 n*M* in the endothelium, which is an increase of 7% over the base case; the steady-state NO concentration in the vascular wall is 69.4 n*M*.

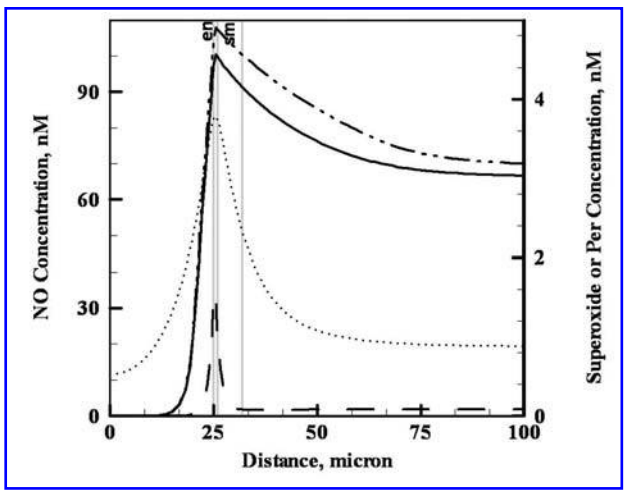

FIG. 3. NO, O_2^-, and Per concentration profiles, base case. Profiles are shown for a 50-mm-diameter arteriole with a luminal RBC-rich region NO-RBC reaction rate of 1,270 per second. Superoxide production is assumed at 20% of the NO production.

Effect of model parameters

We investigated the effect of model parameters including SOD and CO_2 concentrations, NO and O_2^- reaction-rate constant, and no tissue superoxide production on NO, O_2^-, and Per concentration profiles in the tissue. Figure 4 shows the resulting profiles. The common features of these profiles are that (a) the maximal concentrations of these species are in the endothelium, and (b) NO, O_2^-, and peroxynitrite reach steady state in the vascular wall. The effects of individual parameter on the NO, O_2^-, and peroxynitrite concentration profiles with comparison to the base-case profiles are described later.

Superoxide dismutase competes with NO for superoxide and decreases peroxynitrite formation. To evaluate the effect of SOD availability on NO, O_2^-, and peroxynitrite concentrations, SOD concentration was reduced to 0.1 μ*M* as compared with 1 μ*M* in the base case. The calculated concentration profiles are shown in Fig. 4 (dashed curve). The maximum concentrations of NO, O_2^-, and Per are 87.9, 3.0, and 9.8 n*M*, respectively. The reduction in SOD concentration increased the maximum O_2^- and Per concentrations by 100 and 160%, respectively over the base case. On contrary, the maximum NO concentration decreased by 13%. The NO, O_2^-, and Per concentrations are 59.5, 0.3, and 2.9 n*M*, respectively, in the vascular wall.

The importance of CO_2 in this free radical transport model is to scavenge peroxynitrite. For the base case, a CO_2 concentration of 1.14 m*M* was used in the lumen and in the vascular wall. To demonstrate the effect of reduction in CO_2 level on peroxynitrite concentration, we reduced CO_2 concentration to 0.114 m*M*. The NO, O_2^-, and Per concentration profiles are shown in Fig. 4 (dotted curves) for the reduced CO_2 level. The NO and O_2^- concentrations are the same as the base-case concentrations. However, peroxynitrite concentration increases significantly. Peroxynitrite concentrations are 15.8, 6.6, and 11.6 n*M*, respectively, in the endothelium, in the vascular wall, and at the center of lumen; these levels correspond to four-, seven-, and 23-fold increases over the base-case concentrations at the respective locations.

The concentration profiles simulated by using a higher NO and O_2^- reaction-rate constant of 1.6×10^{10} $M^{-1}s^{-1}$ are represented by the dashed-dot-dot curves in Fig. 4. The maximum NO and O_2^- concentrations are 95.4 and 1.3 n*M*, respectively, similar to the base-case concentrations. The maximum Per concentration increases to 6.4 n*M*, an increase of ~70%. The NO, O_2^-, and Per concentrations are 64, 0.1, and 1.6 n*M*, respectively in the vascular wall.

We also considered O_2^- production only in the arteriolar endothelium. The resulting concentration profiles are represented by the solid curves in Fig. 4. The maximum NO, O_2^-, and Per concentrations are 104, 1.5, and 3.2 n*M*, respectively, which is similar to the base-case concentrations. Note that the O_2^- and Per concentrations decrease to zero rapidly in the vascular wall. The O_2^- concentration is decreased from 1.5 n*M* to <0.1 n*M* within 4 μm from its source of production in the arteriolar endothelium, whereas Per concentration is decreased to <0.1 n*M* over a 25-μm distance.

Effect of location of tissue oxidative stress

We investigated the effect of enhancement of O_2^- production in the microcirculation. We increased the endothelium O_2^- to NO release ratio from 0.2 to 2, resulting in the total arteriolar endothelium O_2^- production of 10.6×10^{-12} mol $cm^{-2}s^{-1}$ and perfused-parenchymal tissue O_2^- production of 17.2×10^{-7} M/s. In all other regions, O_2^- production was the same as the base case. The concentration profiles are shown in Fig. 5 (solid curve). The O_2^- and Per profiles drop in the smooth muscle and nonperfused parenchymal regions, because the O_2^- production in the smooth muscle and the nonperfused parenchymal tissue regions is low in comparison to

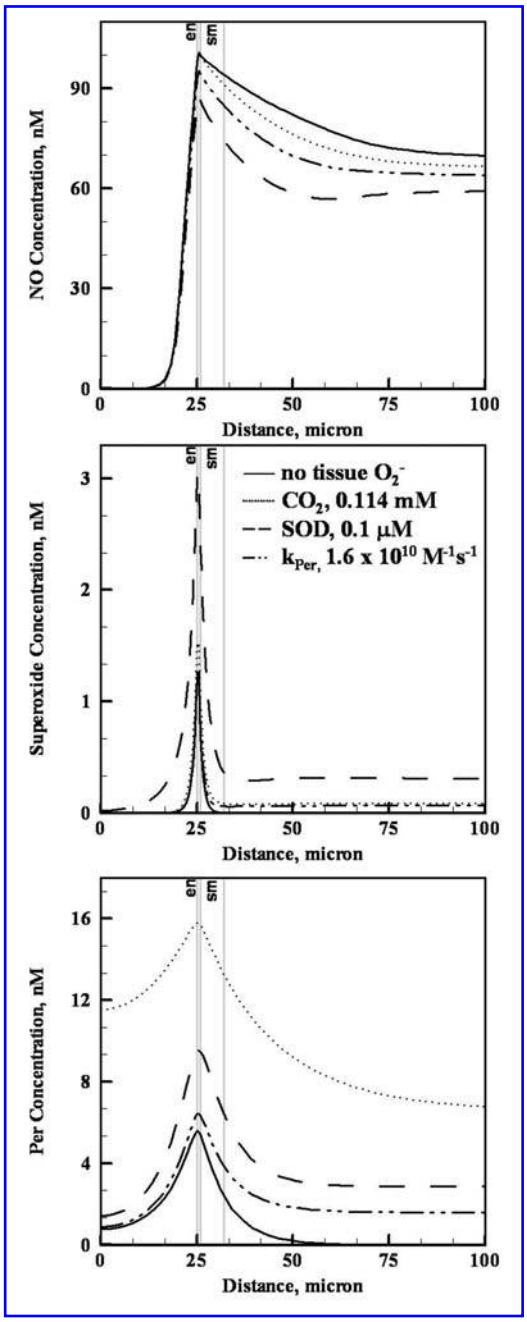

FIG. 4. Effect of parameters on NO, O_2^- and Per concentration profiles. Concentration profiles are shown for varying one model parameter at a time. Model parameters varied are SOD and CO_2 concentrations, NO and O_2^- reaction-rate constant, and no tissue superoxide production.

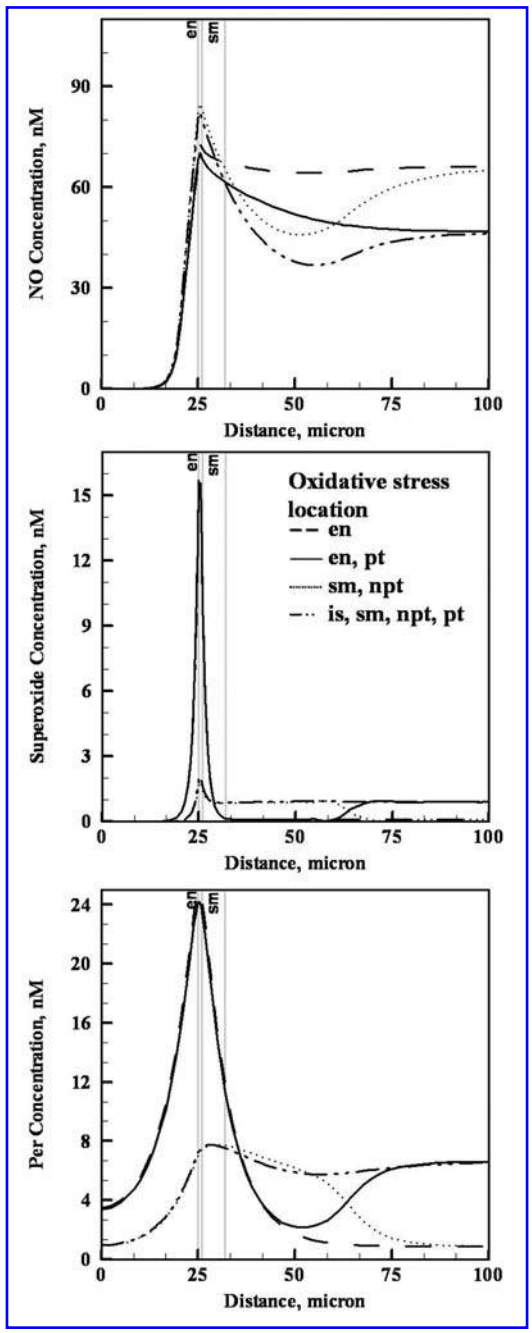

FIG. 5. Effect of location of excess superoxide in oxidative stress on NO, O_2^-, and Per concentration profiles. Depending on a disease condition, the vascular location of excessive superoxide can be in the endothelium, the smooth muscle cell, and the media and adventitia. Concentration profiles are shown for systematic change in the location of excessive oxidative stress to the arteriolar endothelium (en), the arteriolar and capillary endothelium (en, pt), the smooth muscle and the nonperfused parenchymal tissue regions (sm, npt), and every region except arteriolar endothelium (is, sm, npt, pt).

the endothelium and the perfused-parenchymal regions O_2^- production. The maximum NO, O_2^-, and Per concentrations are 70, 15.6, and 24.1 n*M*, respectively, in the endothelium. In the vascular wall, the NO, O_2^-, and Per concentrations are 47, 0.9, and 6.6 n*M*, respectively. With the increased-endothelial cell O_2^- production, the NO concentrations are reduced by 30% as compared with the base-case NO concentrations in the endothelium, smooth muscle, and perfused-parenchymal tissue regions. Conversely, the O_2^- and Per concentrations are increased over nine- and sixfold, respectively, as compared with the base-case concentrations.

We further investigated the importance of regional differences in superoxide production in the vessel wall. For this purpose, we systematically changed the location of excessive oxidative stress to the arteriolar endothelium, to the smooth muscle and the nonperfused parenchymal tissue regions, and to every region except arteriolar endothelium. For O_2^- production in the arteriolar endothelium only, the total arteriolar endothelium O_2^- production of 10.6×10^{-12} mol $cm^{-2}s^{-1}$ was assumed. In all other regions, O_2^- production was the same as in the base case. The concentration profiles are shown as the dashed curve in Fig. 5. The maximum NO, O_2^-, and Per concentrations are 73, 15.5, and 25 n*M*, respectively, in the endothelium. The perfused-parenchymal tissue NO, O_2^-, and Per concentrations remain unchanged from the base-case concentrations.

For excessive O_2^- production in the smooth muscle and the nonperfused parenchymal tissue regions, the O_2^- production of 17.2×10^{-7} M/s was assumed. The concentration profiles are shown as the dotted curve in Fig. 5. The NO, O_2^-, and Per concentrations are 85, 1.8, and 7.3 n*M*, respectively, in the endothelium. The smooth muscle concentration of NO decreased by 22%, peroxynitrite increased by 150%, and O_2^- increased <1 n*M* over the respective base-case concentrations. The perfused-parenchymal tissue NO, O_2^-, and Per concentrations remain unchanged from the base case. For excessive O_2^- production in every region except arteriolar endothelium (dashed-dot-dot curves in Fig. 5), the NO concentrations are reduced up to 45% of the base-case NO concentrations. Conversely, O_2^- and Per concentrations are increased more than nine- and sixfold, respectively, as compared with the base-case concentrations.

DISCUSSION

The aims of the model were (a) to calculate the NO, O_2^-, and peroxynitrite concentrations in and around an arteriolar vessel, and (b) to understand the effects of O_2^- production sites and rates on NO and peroxynitrite concentration in the vascular wall.

NO, O_2^-, and peroxynitrite predictions

Results from this and an earlier model (4) established that the NO, O_2^-, and peroxynitrite concentration gradients are steep in the vascular wall. A number of techniques including microelectrodes and fluorescent and chemiluminescent dyes (43) have been used to measure these free radical levels in various regions of microvessels. Even though great advances have been made in free radical measurements, the spatial resolution of the methods has not been sufficient to measure these steep gradients.

In the base case, inclusion of O_2^- and peroxynitrite interactions with NO did not significantly affect NO levels (Fig. 3), and the NO concentration predictions from this model are consistent with those of other NO-transport models (20, 25, 46). The predicted NO concentrations change <13% for a significant change in parameters values of SOD and CO_2 concentration, NO and O_2^- reaction rate, and no superoxide production in tissue (Fig. 3). For these parameters, the predicted O_2^- concentrations vary between 0 and 3 n*M*. Conversely, the predicted peroxynitrite concentrations can vary significantly between 0 and 16 n*M* and up to 25-fold, depending on a parameter. More experimental and theoretical studies would be required to provide accurate levels of these free radicals in and around an arteriolar vessel.

Effect of superoxide dismutase

Local mechanisms of O_2^- consumption play a major role in (a) superoxide-mediated cytotoxicity, (b) NO bioavailability in blood vessels, and (c) peroxynitrite formation. Thus, the local concentration of SOD can be a key determinant in O_2^- levels. With SOD-deficient genetically altered animals, experimental studies reported that SOD deficiency results in reduced NO bioavailability and increased O_2^- and peroxynitrite levels (8, 18, 51). When the SOD level was decreased in the present study (Fig. 4), the model predictions of increase in O_2^- and Per concentrations by 100% and 160%, respectively, and decrease in NO concentration decreased by 13% are consistent with these experimental observations. Mathematical models that incorporate detailed descriptions of several isoforms of SOD in vascular cells will be useful in enhancing our understanding of the contribution of SOD in the regulation of vascular function.

Pathologic conditions: implication for oxidative stress–related reduced NO bioavailability

NO-mediated vasodilation is attenuated in diabetes, aging, cardiovascular diseases, and hypertension, which may be a result of excessive superoxide formation (12, 40, 42). The vascular location of excessive superoxide can be in the endothelium, the smooth muscle cell, and the media and adventitia in these conditions (5, 30, 49). As we changed the location of excessive superoxide in the microcirculation, the model predictions of NO, O_2^-, and peroxynitrite concentration varied significantly (Fig. 5). Of all the locations for excessive O_2^- release, the excessive O_2^- release in the endothelium results in the maximal decrease in predicted NO concentrations but the maximal increase in peroxynitrite concentrations. Inclusion of excessive O_2^- release in smooth muscle and parenchymal tissue results in significantly low levels of NO and significantly high levels of O_2^- and peroxynitrite in these regions.

PERSPECTIVE

The predictions of the present model support the importance of O_2^- as a local signaling molecule in the vasculature.

Results suggest that the reduced NO bioavailability and enhanced peroxynitrite formation in the microcirculation may vary depending on the location of oxidative stress. Therefore, nitrosylation of membrane proteins and oxidization of lipids may occur at diverse vascular cell locations in diabetes, aging, and cardiovascular diseases. In addition to impairment of NO-dependent vasodilation, peroxynitrite also can inhibit key enzymes and proteins such as prostacyclin synthase (28, 53) in vascular cells. The model results emphasize the need for careful experiments at the individual vascular-wall cell layer for oxidative-stress studies in the vasculature.

In conclusion, we have developed a model to assess the biochemical interactions of NO, O_2^-, and peroxynitrite in the microcirculation. The model results suggest that the transport of these free radicals is significantly affected in oxidative-stress conditions. We predict that the tissue concentrations of NO and peroxynitrite are affected over a larger distance from the location of excessive superoxide formation, even though the superoxide concentrations are reduced to significantly low levels within 2 mm from its production site. These results will have significant implications for our understanding of changes in tissue NO levels in physiologic conditions and mechanisms of reduction in vascular NO levels in endothelial dysfunction.

ACKNOWLEDGMENTS

This work was supported by American Heart Association SDG 0530050N, and Arkansas Biosciences Institute (ABI).

ABBREVIATIONS

eNOS, Endothelial nitric oxide synthase; NO, nitric oxide; NOS, nitric oxide synthase; $ONOO^-$, peroxynitrite anion; ROS, reactive oxygen species; RNS, reactive nitrogen species; RBCs, red blood cells; sGC, soluble guanylate cyclase; O_2^-, superoxide; SOD, superoxide dismutase.

REFERENCES

1. Alderton WK, Cooper CE, and Knowles RG. Nitric oxide synthases: structure, function and inhibition. *Biochem J* 357: 593–615, 2001.
2. Beckman JS and Koppenol WH. Nitric oxide, superoxide, and peroxynitrite: The good, the bad, and ugly. *Am J Physiol* 271: C1424–C1437, 1996.
3. Bellamy TC, Wood J, and Garthwaite J. On the activation of soluble guanylyl cyclase by nitric oxide. *Proc Natl Acad Sci U S A* 99: 507–510, 2002.
4. Buerk DG, Lamkin-Kennard K, and Jaron D. Modeling the influence of superoxide dismutase on superoxide and nitric oxide interactions, including reversible inhibition of oxygen consumption. *Free Radic Biol Med* 34: 1488–1503, 2003.
5. Cai H and Harrison DG. Endothelial dysfunction in cardiovascular diseases: the role of oxidant stress. *Circ Res* 87: 840–844, 2000.
6. Carlsen E and Comroe JH Jr. The rate of uptake of carbon monoxide and of nitric oxide by normal human erythrocytes and experimentally produced spherocytes. *J Gen Physiol* 42: 83–107, 1958.
7. Condorelli P and George SC. In vivo control of soluble guanylate cyclase activation by nitric oxide: a kinetic analysis. *Biophys J* 80: 2110–2119, 2001.
8. Cooke CL and Davidge ST. Endothelial-dependent vasodilation is reduced in mesenteric arteries from superoxide dismutase knockout mice. *Cardiovasc Res* 60: 635–642, 2003.
9. Droge W. Free radicals in the physiological control of cell function. *Physiol Rev* 82: 47–95, 2002.
10. d'Uscio LV, Milstien S, Richardson D, Smith L, and Katusic ZS. Long-term vitamin C treatment increases vascular tetrahydrobiopterin levels and nitric oxide synthase activity. *Circ Res* 92: 88–95, 2003.
11. Fridovich I. Superoxide radical and superoxide dismutases. *Annu Rev Biochem* 64: 97–112, 1995.
12. Griendling KK, Sorescu D, and Ushio-Fukai M. NAD(P)H oxidase: role in cardiovascular biology and disease. *Circ Res* 86: 494–501, 2000.
13. Griffith OW and Stuehr DJ. Nitric oxide synthases: properties and catalytic mechanism. *Annu Rev Physiol* 57: 707–736, 1995.
14. Guzik TJ, Mussa S, Gastaldi D, Sadowski J, Ratnatunga C, Pillai R, and Channon KM. Mechanisms of increased vascular superoxide production in human diabetes mellitus: role of NAD(P)H oxidase and endothelial nitric oxide synthase. *Circulation* 105: 1656–1662, 2002.
15. Haas TL and Duling BR. Morphology favors an endothelial cell pathway for longitudinal conduction within arterioles. *Microvasc Res* 53: 113–120, 1997.
16. Huie RE and Padmaja S. The reaction of no with superoxide. *Free Radic Res Commun* 18: 195–199, 1993.
17. Ignarro LJ. Signal transduction mechanisms involving nitric oxide. *Biochem Pharmacol* 41: 485–490, 1991.
18. Jung O, Marklund SL, Geiger H, Pedrazzini T, Busse R, and Brandes RP. Extracellular superoxide dismutase is a major determinant of nitric oxide bioavailability: in vivo and ex vivo evidence from ecSOD-deficient mice. *Circ Res* 93: 622–629, 2003.
19. Kavdia M and Lewis RS. Free radical profiles in an encapsulated pancreatic cell matrix model. *Ann Biomed Eng* 30: 721–730, 2002.
20. Kavdia M and Popel AS. Contribution of nNOS- and eNOS-derived NO to microvascular smooth muscle NO exposure. *J Appl Physiol* 97: 293–301, 2004.
21. Kavdia M and Popel AS. Wall shear stress differentially affects NO level in arterioles for volume expanders and Hb-based O2 carriers. *Microvasc Res* 66: 49–58, 2003.
22. Kavdia M, Tsoukias NM, and Popel AS. Model of nitric oxide diffusion in an arteriole: impact of hemoglobin-based blood substitutes. *Am J Physiol Heart Circ Physiol* 282: H2245–H2253, 2002.
23. Kojda G and Harrison D. Interactions between NO and reactive oxygen species: pathophysiological importance in atherosclerosis, hypertension, diabetes and heart failure. *Cardiovasc Res* 43: 562–571., 1999.
24. Koppenol WH, Moreno JJ, Pryor WA, Ischiropoulos H, and Beckman JS. Peroxynitrite, a cloaked oxidant formed by nitric oxide and superoxide. *Chem Res Toxicol* 5: 834–842, 1992.

25. Lamkin-Kennard KA, Buerk DG, and Jaron D. Interactions between NO and O(2) in the microcirculation: a mathematical analysis. *Microvasc Res* 68: 38–50, 2004.
26. Lewis RS and Deen WM. Kinetics of the reaction of nitric oxide with oxygen in aqueous solutions. *Chem Res Toxicol* 7: 568–574, 1994.
27. Liochev SI and Fridovich I. Superoxide and nitric oxide: consequences of varying rates of production and consumption: a theoretical treatment. *Free Radic Biol Med* 33: 137–141, 2002.
28. Liu Y, Terata K, Chai Q, Li H, Kleinman LH, and Gutterman DD. Peroxynitrite inhibits Ca2+-activated K+ channel activity in smooth muscle of human coronary arterioles. *Circ Res* 91: 1070–1076, 2002.
29. Malinski T, Taha Z, Grunfeld S, Patton S, Kapturczak M, and Tomboulian P. Diffusion of nitric oxide in the aorta wall monitored in situ by porphyrinic microsensors. *Biochem Biophys Res Commun* 193: 1076–1082, 1993.
30. Miller FJ Jr, Gutterman DD, Rios CD, Heistad DD, and Davidson BL. Superoxide production in vascular smooth muscle contributes to oxidative stress and impaired relaxation in atherosclerosis. *Circ Res* 82: 1298–1305, 1998.
31. Moncada S, Palmer RM, and Higgs EA. Nitric oxide: physiology, pathophysiology, and pharmacology. *Pharmacol Rev* 43: 109–142, 1991.
32. Nalwaya N and Deen WM. Analysis of cellular exposure to peroxynitrite in suspension cultures. *Chem Res Toxicol* 16: 920–932, 2003.
33. Nalwaya N and Deen WM. Peroxynitrite exposure of cells cocultured with macrophages. *Ann Biomed Eng* 32: 664–676, 2004.
34. Pfeiffer S, Gorren AC, Schmidt K, Werner ER, Hansert B, Bohle DS, and Mayer B. Metabolic fate of peroxynitrite in aqueous solution: reaction with nitric oxide and pH-dependent decomposition to nitrite and oxygen in a 2:1 stoichiometry. *J Biol Chem* 272: 3465–3470, 1997.
35. Pfeiffer S, Schmidt K, and Mayer B. Dityrosine formation outcompetes tyrosine nitration at low steady-state concentrations of peroxynitrite: Implications for tyrosine modification by nitric oxide/superoxide in vivo. *J Biol Chem* 275: 6346–6352, 2000.
36. Popel AS. Theory of oxygen transport to tissue. *Crit Rev Biomed Eng* 17: 257–321, 1989.
37. Radi R. Peroxynitrite reactions and diffusion in biology. *Chem Res Toxicol* 11: 720–721, 1998.
38. Rajagopalan S, Kurz S, Munzel T, Tarpey M, Freeman BA, Griendling KK, and Harrison DG. Angiotensin II-mediated hypertension in the rat increases vascular superoxide production via membrane NADH/NADPH oxidase activation: contribution to alterations of vasomotor tone. *J Clin Invest* 97: 1916–1923, 1996.
39. Salgo MG, Bermudez E, Squadrito G L, and Pryor WA. DNA damage and oxidation of thiols peroxynitrite causes in rat thymocytes. *Arch Biochem Biophys* 322: 500–505, 1995.
40. Schulz E, Anter E, and Keaney JF, Jr. Oxidative stress, antioxidants, and endothelial function. *Curr Med Chem* 11: 1093–1104, 2004.
41. Sharan M and Popel AS. A two-phase model for flow of blood in narrow tubes with increased effective viscosity near the wall. *Biorheology* 38: 415–428, 2001.
42. Sun D, Huang A, Yan EH, Wu Z, Yan C, Kaminski PM, Oury TD, Wolin MS, and Kaley G. Reduced release of nitric oxide to shear stress in mesenteric arteries of aged rats. *Am J Physiol Heart Circ Physiol* 286: H2249–H2256, 2004.
43. Tarpey MM, Wink DA, and Grisham MB. Methods for detection of reactive metabolites of oxygen and nitrogen: in vitro and in vivo considerations. *Am J Physiol Regul Integr Comp Physiol* 286: R431–R444, 2004.
44. Tsoukias NM, Kavdia M, and Popel AS. A theoretical model of nitric oxide transport in arterioles: Frequency vs amplitude dependent control of cGMP formation. *Am J Physiol Heart Circ Physiol* 286: H1043–H1056, 2004.
45. Vasquez-Vivar J, Kalyanaraman B, Martasek P, Hogg N, Masters BS, Karoui H, Tordo P, and Pritchard KA, Jr. Superoxide generation by endothelial nitric oxide synthase: the influence of cofactors. *Proc Natl Acad Sci U S A* 95: 9220–9225, 1998.
46. Vaughn MW, Kuo L, and Liao JC. Effective diffusion distance of nitric oxide in the microcirculation. *Am J Physiol* 274: H1705–H1714, 1998.
47. Vaughn MW, Kuo L, and Liao JC. Estimation of nitric oxide production and reaction rates in tissue by use of a mathematical model. *Am J Physiol* 274: H2163–H2176, 1998.
48. Walmsley JG, Gore RW, Dacey RG, Jr., Damon DN, and Duling BR. Quantitative morphology of arterioles from the hamster cheek pouch related to mechanical analysis. *Microvasc Res* 24: 249–271, 1982.
49. Wang HD, Pagano PJ, Du Y, Cayatte AJ, Quinn MT, Brecher P, and Cohen RA. Superoxide anion from the adventitia of the rat thoracic aorta inactivates nitric oxide. *Circ Res* 82: 810–818, 1998.
50. White CR, Darley-Usmar V, Berrington WR, McAdams M, Gore JZ, Thompson JA, Parks DA, Tarpey MM, and Freeman BA. Circulating plasma xanthine oxidase contributes to vascular dysfunction in hypercholesterolemic rabbits. *Proc Natl Acad Sci U S A* 93: 8745–8749, 1996.
51. Yan C, Huang A, Wu Z, Kaminski PM, Wolin MS, Hintze TH, Kaley G, and Sun D. Increased superoxide leads to decreased flow-induced dilation in resistance arteries of Mn-SOD-deficient mice. *Am J Physiol Heart Circ Physiol* 288: H2225–H2231, 2005.
52. Zacharia IG and Deen WM. Diffusivity and solubility of nitric oxide in water and saline. *Ann Biomed Eng* 33: 214–222, 2005.
53. Zou MH and Ullrich V. Peroxynitrite formed by simultaneous generation of nitric oxide and superoxide selectively inhibits bovine aortic prostacyclin synthase. *FEBS Lett* 382: 101–104, 1996.

Address reprint requests to:
Mahendra Kavdia, Ph.D.
Biomedical Engineering Program
203, Engineering Hall
University of Arkansas
Fayetteville, AR 72701

E-mail: mkavdia@uark.edu

Date of first submission to ARS Central, December 29, 2005; date of acceptance, January 22, 2006.

This article has been cited by:

1. Saptarshi Kar, Bhagyesh Bhandar, Mahendra Kavdia. 2012. Impact of SOD in eNOS uncoupling: a two-edged sword between hydrogen peroxide and peroxynitrite. *Free Radical Research* 1-40. [CrossRef]
2. Prabhakar Deonikar, Mahendra Kavdia. 2010. An Integrated Computational and Experimental Model of Nitric Oxide–Red Blood Cell Interactions. *Annals of Biomedical Engineering* **38**:2, 357-370. [CrossRef]
3. Prabhakar Deonikar, Mahendra Kavdia. 2010. Extracellular diffusion and permeability effects on NO–RBCs interactions using an experimental and theoretical model. *Microvascular Research* **79**:1, 47-55. [CrossRef]
4. Michalis G. Nikolaidis, Athanasios Z. Jamurtas. 2009. Blood as a reactive species generator and redox status regulator during exercise. *Archives of Biochemistry and Biophysics* **490**:2, 77-84. [CrossRef]
5. F. Moien-Afshari, S. Ghosh, M. Khazaei, T. J. Kieffer, R. W. Brownsey, I. Laher. 2008. Exercise restores endothelial function independently of weight loss or hyperglycaemic status in db/db mice. *Diabetologia* **51**:7, 1327-1337. [CrossRef]
6. Kejing Chen , Roland N. Pittman , Aleksander S. Popel . 2007. Vascular Smooth Muscle NO Exposure from Intraerythrocytic SNOHb: A Mathematical Model. *Antioxidants & Redox Signaling* **9**:8, 1097-1110. [Abstract] [Full Text PDF] [Full Text PDF with Links]
7. Stefan I. Liochev, Irwin Fridovich. 2007. The effects of superoxide dismutase on H2O2 formation. *Free Radical Biology and Medicine* **42**:10, 1465-1469. [CrossRef]